HHS Public Access

Author manuscript

*Biochem J.* Author manuscript; available in PMC 2021 December 11.

Published in final edited form as:

*Biochem J.* 2020 December 11; 477(23): 4515–4526. doi:10.1042/BCJ20200671.

# The biophysical basis of receptor tyrosine kinase ligand functional selectivity: Trk-B case study

**Fozia Ahmed**[1,3], **Michael D. Paul**[2,3], **Kalina Hristova**[1,2,3,*]

[1]Department of Materials Science and Engineering, Johns Hopkins University, 3400 Charles Street, Baltimore, MD 21218

[2]Program in Molecular Biophysics and Johns Hopkins University, 3400 Charles Street, Baltimore, MD 21218

[3]Institute for NanoBioTechnology, Johns Hopkins University, 3400 Charles Street, Baltimore, MD 21218

## Abstract

Tropomyosin receptor kinase B (Trk-B) belongs to the second largest family of membrane receptors, Receptor Tyrosine Kinases (RTKs). Trk-B is known to interact with three different neurotrophins: Brain-Derived Neurotrophic Factor (BDNF), Neurotrophin-4 (NT-4), and Neurotrophin-3 (NT-3). All three neurotrophins are involved in survival and proliferation of neuronal cells, but each induces distinct signaling through Trk-B. We hypothesize that the different biological effects correlate with differences in the interactions between the Trk-B receptors, when bound to different ligands, in the plasma membrane. To test this hypothesis, we use quantitative FRET to characterize Trk-B dimerization in response to NT-3 and NT-4 in live cells, and compare it to the previously published data for Trk-B in the absence and presence of BDNF. Our study reveals that the distinct Trk-B signaling outcomes are underpinned by *both* different configurations and different stabilities of the three ligand-bound Trk-B dimers in the plasma membrane.

## Introduction

Receptors in the plasma membrane can bind multiple ligands, and can initiate multiple downstream signaling cascades that control cellular physiology in health and disease (1–3). Recent work has uncovered that different ligands can lead to different biological outcomes while acting through the same receptor. This phenomenon is known as “ligand bias” or “ligand functional selectivity,” and has been extensively characterized for the largest family of membrane receptors, the seven helix G-protein coupled receptors (GPCRs) (4–6). The mechanism of ligand bias in GPCR signaling is now established: different GPCR ligands stabilize different functional receptor conformations, and each of the conformations only efficiently triggers a subset of the possible downstream signaling cascades (7–9). The discovery and the mechanistic studies of GPCR bias have redefined fundamental concepts in

* kh@jhu.edu.

**Author contributions**: F.A. performed the FRET experiments. M.P. performed the N&B experiments. F.A., M.P. and K.H. analyzed the data and wrote the paper.

pharmacology, and have opened up new possibilities for the development of more effective and specific therapeutics (10–13).

While most ligand bias investigations have focused on the GPCRs, ligand bias has also been reported for the second largest family of membrane receptors, the receptor tyrosine kinases (RTKs) (1,3,14–16). RTKs are single-pass transmembrane proteins that control cell growth, differentiation, motility, and metabolism (17,18), by transducing biochemical signals via lateral dimerization or oligomerization in the plasma membrane. Their N-terminal extracellular (EC) ligand-binding regions are composed of characteristic structural domains (19). They also have single transmembrane helices and intracellular kinase domains (Fig. 1). The cross-phosphorylation of two kinase domains in the ligand-bound dimers and oligomers stimulates catalytic activity, triggering downstream signaling cascades that control cell behavior (18,20–22).

There are reports of ligand bias involving different RTKs (1), including the ERBB receptors (23), the fibroblast growth factor receptors (FGFRs) (24), the Eph receptors (25), and the insulin receptor (26,27). However, the mechanism behind this ligand bias is not well understood for the RTKs, and is a subject of debate. Some studies have proposed that RTK ligand bias occurs through a mechanism that is analogous to the one used by the GPCRs, i.e., different RTK ligands stabilize different RTK dimer configurations, leading to differential kinase domain activity (15). Others, however, argue that the mechanism is fundamentally different, as RTK kinase domains cannot sense the identity of the bound ligand because the linkers between the different RTK domains are flexible (16,28,29). Instead, these researchers propose that the stability of the RTK dimer is the important parameter that controls ligand bias (16,30).

Here, we investigate the biophysical basis behind biased signaling by Trk-B, an RTK that belongs to the three-member Tropomyosin receptor kinases (Trks) subfamily. This subfamily is characterized by extracellular domains that contain three tandem leucine rich repeats flanked by cysteine rich domains and two immuoglobulin-like domains (31–34). The Trk receptors initiate signaling cascades that control neuronal cell survival and proliferation, axonal and dendritic growth, as well as synaptic connections and synaptic plasticity (33,35–37). Trk-B, studied here, is the most prominently expressed Trk receptor in the brain, and it plays a vital role in neural plasticity in early central nervous system development and in adulthood (38–42). Trk-B signals in response to three different neurotrophins, BDNF, NT-3 and NT-4, which are small biological molecules with 50% sequence identity (43–45).

These three neurotrophin ligands have been reported to have similar binding affinities to Trk-B (44,46–48). However, they can lead to different cellular responses when signaling through Trk-B. BDNF has been shown to play a more substantial role than NT-4 in synaptic transmission and plasticity and in higher cognitive functions (49). On the other hand, NT-4 has a larger role in inducing neuronal survival and synaptic maturation (50,51). Moreover, in NIH 3T3 cells, both BDNF and NT-4 initiate growth responses more strongly than NT-3 (46,52,53). Based on the mechanism of ligand bias in GPCRs, it is possible that the conformations of the different neurotrophin-bound Trk-B dimers in the plasma membrane

are different. It is also possible that the stabilities of the three ligand-bound Trk-B dimers are different.

We have previously established a FRET assay that can yield RTK association constants and can report on the occurrence of conformational changes in the RTK dimer upon ligand binding (54–56). Using this assay, we have shown that Trk-B forms a dimer of high stability ($K_{diss}$ = 12 ± 2 rec/μm$^2$), even in the absence of ligand (56). The binding of BDNF to the pre-formed Trk-B dimer triggers a conformational change in the dimer, and further enhances its stability (56). Here, we investigate the response of Trk-B to NT-3 and NT-4, in order to compare it to the response to BDNF and gain insight into the biophysical basis of ligand functional selectivity.

## Materials and Methods

### Plasmids

The pDNR-Dual Trk-B plasmid (# HsCD00022371) was purchased from DNASU Plasmid Respository. The Trk-B gene was cloned into the pcDNA 3.1+ vector, containing a $(GGS)_5$ linker followed by a fluorescent protein (either mTurquoise or YFP). Cloning was done using the Gibson assembly kit (NEBuilder HiFI DNA assembly, New England Biolabs, E5520S), as described previously (56). The extracellular + transmembrane (ECTM) (no kinase domain) version of Trk-B was cloned similarly (56).

### Cell culture and transfection for HEK293T cells

Human embryonic kidney cells (HEK293T) were purchased from ATCC. HEK293T were kept at 37$^0$C in the presence of 5% $CO_2$ and cultured in Dulbecco's Modified Eagle Media (DMEM, ThermoFisher Scientific, 31600034) supplemented with 10% fetal bovine serum (FBS, Hylone, SH30070.03). Prior to imaging, the cells were seeded on collagen coated dishes (MatTek, P35GCOL-1.5-14-C) at a density of 2.5*10$^5$ cells/dish. For the FRET experiments, these cells were transfected approximately 24 hours after seeding with a total of 2 ug of DNA using Fugene HD (Promega, E2311) according to the manufacturer's protocol. The medium was changed to serum free medium approximately 12 hours before image acquisition to remove all traces of endogenous ligands.

Cells that were singly transfected with either Trk-B-mTurquoise or Trk-B-YFP served as controls. For the FRET experiments, cells were co-transfected with 1:3 Trk-B-mTruquoise: Trk-B-YFP. The emission spectra of co-transfected cells were deconvoluted into the mTurquoise (donor) and YFP (acceptor) spectra, as determined using the singly transfected control cells (54). Purified soluble mTurquoise and YFP were used as solution standards to convert intensities of the fluorophores into concentrations (54). The soluble fluorescent proteins were purified from bacteria, as described previously (57).

### Image acquisition and analysis for FSI-FRET

HEK293T cells were subjected to reversible osmotic stress in hypoosmotic media containing 1:9 serum-free media: di$H_2O$, 25mM HEPES. This procedure removes the "ruffles" or "folds" of the membrane (58), enabling accurate quantification of the donor and acceptor

concentrations (58). Human brain-derived neurotrophic factor (BDNF, Cell Signaling Technology, 3897S), human neurotrophin-3 (NT-3, Cell Signaling Technology, 5237SC), human neurotrophin-4 (NT-4, Peprotech) were added at a concentration of ~5ug/mL (380 nM) in the hypotonic media, at the time of imaging. Cells were allowed to equilibrate for 10 mins before imaging, and each dish was imaged for ~ 2 hours.

Complete emission spectra were acquired with a two photon microscope equipped with the OptiMiS detection system. The microscope has line-scan excitation capabilities, and yields fluorescence spectra for each pixel in the image (59). Image analysis was performed using the Fully Quantified Spectral Imaging FRET (FSI-FRET) method (54). This method allows us to determine the two-dimensional donor and acceptor concentrations in the membrane, along with the FRET efficiency. The measured FRET efficiency is corrected for proximity FRET as previously described (60). A monomer-dimer equilibrium model is fit to the data, to determine the two-dimensional dissociation constant ($K_{diss}$) and the structural parameter intrinsic FRET ($\tilde{E}$).

The dimeric fraction is determined from the corrected FRET efficiency, $E$:

$$f_D = \frac{E}{x_A \tilde{E}} \tag{1}$$

The constant $\tilde{E}$ depends on the separation, orientation, and dynamics of the two fluorescent proteins in the dimer (not on the dimerization propensity), and $x_A$ is the acceptor fraction. The dependence of $\tilde{E}$ on the distance between the fluorescent proteins in the dimer, $d$, is given by (60,61)

$$\tilde{\mathrm{E}} = \frac{1}{1 + \left(\frac{d}{R_0}\right)^6} \tag{2}$$

where $R_0$ is the Forster radius for the mTurquoise-eYFP FRET pair, 54.5 Å. This equation assumes free rotation of the fluorescent proteins, an assumption that is justified because the fluorescent proteins are attached to long flexible linkers.

Based on the law of mass action, the dimeric fraction can be written as a function of the total receptor concentration, $T$, and $K_{diss}$:

$$f_D = \frac{1}{T}\left(T - \frac{K_{diss}}{4}\left(\sqrt{1 + 8T/K_{diss}} - 1\right)\right) \tag{3}$$

We use equations (1) and (3) to fit the measured dimeric fractions while optimizing for the two adjustable parameters: $K_{diss}$ and $\tilde{E}$.

The stability of the dimer is related to the dissociation constant according to

$$\Delta G = RT\ln\left(K_{diss}/10^6\right) \quad (4)$$

with $K_{diss}$ reported in units of receptors per μm$^2$, and the standard state for the $\Delta G$ calculation defined as $K^0_{diss} = 1$ rec/nm$^2$ (61).

When the receptors are 100% dimeric ($f_D$=1), equation (1) reduces to

$$E = x_A\widetilde{\mathrm{E}} \quad (5)$$

### Image acquisition and analysis for N&B

HEK293T cells were prepared in an identical fashion as for the FRET experiments, except that the cells were transfected with 1-2 μg of either LAT-mTurquoise, E-cadherin-mTurquoise, or Trk-B-mTurquoise using Lipofectamine 3000 (Invitrogen, L3000008) according to the manufacturer's protocol; the LAT and E-cadherin constructs have previously been described (62,63). The cells were imaged in the starvation media, and 2.5 μg/mL of ligand was added 10 minutes prior to imaging; each dish was imaged for no more than two hours. Imaging was performed using the photon counting mode of a Leica8 confocal microscope. The basolateral membrane of the cells was imaged in order to ensure that the membrane being measured had a relatively flat topology. An image stack of 150 images (256 by 256 pixels each) was collected over approximately 90 seconds (5.4 μs pixel dwell time) using an 18x optical zoom (40.2 nm pixel length). A 488 laser at .1% of max power was used to excite the cells, using the default CFB setting for the emission window.

The image stack of each cell was examined as a video, and cells which were visibly expanding, contracting, or exhibiting membrane deformation were excluded from the analysis. Image analysis was performed in MATLAB using well established protocols (54). In brief, the image stack was aligned to correct for movement using MATLAB's "dftregistration" function (54). A region of interest was then manually selected for analysis, and the brightness value (i.e., the ratio of the variance to the mean fluorescence intensity across the image stack) was calculated for each pixel in the region of interest. If there was any remaining movement or photobleaching, boxcar averaging was instead used to calculate the brightness value (64,65). The mean brightness value for all the pixels in the region of interest was determined, and it was taken as the brightness value for that cell. Since the imaging was performed in a photon counting mode, the molecular brightness, ε, was obtained from the brightness value by subtracting one. Oligomer size scales linearly with ε, and accordingly, the oligomer size was determined by dividing the experimental ε by the ε of the monomer control, LAT.

## RESULTS

We use quantitative FRET to characterize the lateral interactions between Trk-B receptors, labeled with fluorescent proteins at the C-terminus (either mTurquoise or YFP, a FRET pair) via flexible $(GGS)_5$ linkers, in the presence of two ligands, NT-3 and NT-4. Experiments

were conducted in the presence of ~5μg/mL (380nM) NT-3 or NT-4, well above the reported ligand-receptor dissociation constants, which are in the pM to low nM range (44,46–48). The FRET method that we use has been described in detail previously (54,66–68), and is briefly described in Materials and Methods. The experiments yield three parameters: FRET efficiency, donor (TrkB-mTurquoise) concentration, and acceptor (TrkB-YFP) concentration, in small patches of the plasma membrane of live cells. Hundreds of individual cells, all expressing different amounts of Trk-B-mTurquoise and Trk-B-YFP, are analyzed and combined to produce binding curves.

Figures 1A and 1C show the FRET efficiencies in single cells as a function of the acceptor concentration in the presence of NT-3 and NT-4, respectively, while Figures 1B and 1D show the donor concentration as a function of the acceptor concentration in the presence of the two ligands. In Figures 1A and 1C, we also include the proximity FRET, which occurs due to the random close approach (within 100 Å) of the donors and acceptors (60,69,70). The measured FRET has a substantial contribution from proximity FRET due to the receptors being confined to the two-dimensional plasma membrane. The measured FRET is corrected for this proximity contribution following an established protocol that has been previously verified (60).

The corrected FRET, which is due to specific interactions between Trk-B molecules, is shown in Figure 1E as a function of the total concentration. We see that the corrected FRET does not depend on the concentration, which indicates that Trk-B is a constitutive oligomer over the concentration range sampled in our experiments. Similar results were obtained previously in the presence of 380 nM BDNF (56).

It is known that most RTKs signal as dimers, but higher order oligomers have been proposed to form as well (71). We therefore investigated the possibility that the different ligands promote the formation of different size oligomers using Number and Brightness (N&B), a fluorescence fluctuations technique which directly reports on oligomer size (72–74). Results are shown for Trk-B in the absence of ligand and in the presence of the three ligands, as well as for a monomer control, LAT (63), and a dimer control, Ecadherin (62). The mean oligomer size for Trk-B in the absence of ligand is 1.8 ± 0.1. It is 2.2 ± 0.2, 2.1 ± 0.3, and 2.3 ± 0.3 in the presence of NT-3, NT-4, or BDNF, respectively. Thus, we see no indication for the presence of higher order oligomers, and we conclude that ligand-bound Trk-B is always a dimer.

Figure 1E shows the binned dimeric fractions in the presence of the three ligands, as well as the dimeric fraction measured previously in the absence of ligand for Trk-B (dimerization parameters shown in Table 1). In the case of a dimer, the measured FRET in each cell region is proportional to the value of Intrinsic FRET ($\widetilde{E}$), a structural parameter which depends on the positioning and dynamics of the fluorescent proteins attached to the C-termini of the receptors (61,75). $\widetilde{E}$ is calculated using equation (5), and the histograms of Intrinsic FRET values, measured in the individual cells for each receptor/ligand pair, are shown in Figure 1F. Also included in Figure 1E are previously measured $\widetilde{E}$ values for Trk-B in the presence of 380 nM BDNF (56). The three histograms are fit to Gaussians, and the mean and standard errors are shown in Table 1.

There are highly statistically significant differences in the measured $\widetilde{E}$ values in the presence of the three ligands in Table 1, as determined using ANOVA ($p<0.001$). Note that for all ligands, we are interrogating 100% dimeric receptors (Figure 1E), and thus the only difference in the experiments is the identity of the ligand that is bound to the EC domains. Therefore, the results directly demonstrate that there are differences in the conformations of the intracellular domains when the different ligands are bound, resulting in different relative positioning and/or dynamics of the attached fluorescent proteins. In Table 1, we calculate the distance between the fluorescent proteins in the dimers, under the assumption of free fluorescent protein rotation. These distances help us visualize the results, as shown in Figure 1I.

To gain additional insights into the effect of the three ligands on Trk-B dimerization, we performed FRET experiments with a truncated Trk-B construct with deleted kinase domains. This construct contains the extracellular and transmembrane domains of Trk-B (and is thus called “ECTM”), a 15 amino acid flexible $(GGS)_5$ linker, and the fluorescent proteins. In Figure 2A and 2C, we show the FRET efficiencies for the ECTM Trk-B construct in the presence of 380 nM of NT-3 and NT-4, along with the proximity FRET contribution. Figure 2B and 2D show the donor concentration versus the acceptor concentration for each of these cells, in the presence of NT-3 and NT-4. Figure 2E shows the corrected FRET efficiency that is due to specific interactions between the ECTM Trk-B molecules, as a function of the total Trk-B concentration.

Unlike in the case of full-length Trk-B, here the specific FRET increases as a function of the concentration. This indicates that Trk-B monomers and dimers coexist in the plasma membrane, and that the dimer population increases with the concentration as dictated by the law of mass action. A model of monomer-dimer equilibrium, given by equations (1) and (3), was fit to the data in Figure 2E. The two unknown parameters in the fit were the dissociation constant, $K_{diss}$, a measure of the strength of Trk-B interactions in the presence of 380 nM ligand, and the structural parameter Intrinsic FRET. The best-fit $K_{diss}$ and Intrinsic FRET values for ECTM TrkB in the presence of the different ligands are shown in Table 1, along with previous results for the ligand BDNF. Figure 2F shows experimental binned dimeric fractions in the presence of the three ligands, along with the best-fit. For comparison, we also show the ECTM TrkB dimeric fraction in the absence of ligand.

As seen in Figure 2F and in Table 1, the stabilities of the three ligand-bound Trk-B dimers (at 380 nM ligand) are different. Furthermore, the Intrinsic FRET values measured in the presence of the three ligands are different, as determined with ANOVA ($p<0.001$). As the fluorescent proteins are attached to the TM domain C-termini via flexible linkers, these results suggest that the distance between the C-termini of the TM helices are different when different ligands are bound to the EC domain (Figure 2G), indicating that the conformations of the Trk-B TM domain dimer are different. Thus, both the structures and stabilities of the ECTM Trk-B dimers are different when the three different ligands are bound to them.

## DISCUSSION

Two hypotheses have been discussed in the literature to explain the occurrence of RTK ligand bias. According to one hypothesis, ligand bias arises because the conformations of the kinase domain dimers are different when different ligands are bound to the EC domains (76). This hypothesis is based on the assumption that the conformational changes in the EC domain in response to the bound ligand are transmitted along the length of the RTK and reach the kinase domain (77). In support of this view, it has been shown that different ligands, bound to the same RTK, can induce different TM domain dimer conformations, or different conformations of the linker connecting the TM and kinase domains (the juxtamembrane domain) (55,78–80). Yet, there have been no direct demonstrations that the kinase domains can adopt distinct configurations when different ligands are bound to the EC regions. In part, this is due to experimental challenges to assess the conformation of the kinase domains inside cells when different ligands are bound to the EC domain. Here, we overcome the challenges by quantifying the Intrinsic FRET between the fluorescent proteins in the Trk-B dimer (56). We observe differences in the presence of NT-3, NT-4, and BDNF. These observed differences in Intrinsic FRET suggest differences in the relative positioning and/or dynamics of the fluorescent proteins, and therefore of the Trk-B domains to which the fluorescent proteins are attached.

RTKs first cross-phosphorylate each other on tyrosines in the activation loops of the kinases, which significantly increases the activity of the kinases. Afterwards, the kinases phosphorylate additional tyrosines in the intracellular domains, which serve as binding sites for effector proteins. For phosphorylation to occur, the kinase domains must interact with each other such that each of these tyrosines finds itself in close proximity to the active site of the neighboring kinase. Since multiple phosphorylation events need to take place, the two kinases in the dimer presumably interact through several different interfaces. There are crystal structures of isolated kinase domain dimers that are believed to be snapshots of specific phosphorylation events (81–85); these structures attest to the fact that different kinase dimers can form to enable phosphorylation of different tyrosines. Each different kinase dimer configuration likely positions the fluorescent proteins attached to the C-terminus of full-length TrkB at a certain average distance from each other. If the kinases explore multiple dimer configurations, the measured FRET efficiency in our experiments will be a weighted average of the FRET for each specific dimer configuration. The weights will be determined by the relative amounts of time spent in each of these configurations.

If the hypothesis that different ligands differentially stabilize different kinase dimer configurations holds true, then the weights with which the different ligand-bound configurations contribute to FRET will be different, and so will be the measured FRET for full-length TrkB, when bound to different ligands. This is exactly what we observe here. Thus, our data support the idea that the information about the identity of the bound ligand is transmitted from the EC domain to the kinase domain.

Since the TM domain provides the structural link between the EC ligand-binding domain and the intracellular kinase domain, it has been hypothesized that the TM domains sense the identities of the bound ligands and, as a result, adopt different dimer configurations

(55,77,78). Our data are consistent with this view, as we measure different Intrinsic FRET values for the ECTM TrkB dimers bound to the three different ligands. As the fluorescent proteins are attached to the TM C-termini via flexible linkers, we interpret the different Intrinsic FRET values as an indication that the separation between the TM C-termini is different when different ligands are bound. Taken together, the different Intrinsic FRET values measured for full-length TrkB and ECTM TrkB suggest that NT-3, NT-4, and BDNF differentially stabilize different TrkB dimer configurations. The exact structural differences, however, are unknown.

A second hypothesis has been proposed in the literature to explain the occurrence of ligand bias, prompted in part by observations that the EC and IC domains in RTKs can change conformations independent of each other, and thus are not strongly coupled (16,28,29). It states that the differential engagement of signaling cascades in response to different ligands is correlated with the thermodynamic stabilities of the ligand-bound RTK dimers in the plasma membrane (16,30). To test this hypothesis, we sought to compare the thermodynamic stability of Trk-B dimers at saturating concentrations of NT-3, NT-4, and BDNF. While we could not measure the thermodynamic stability for full-length ligand-bound Trk-B because it was 100% dimeric in our experiment, the stability of the ECTM Trk-B dimer was measurable due to the loss of favorable stabilizing contacts between the Trk-B kinase domains (as demonstrated previously (56)). We were thus able to compare the thermodynamic stabilities of the three ECTM Trk-B dimers, and we observed distinct differences among them. Accordingly, our data are consistent with the idea that the biased ligands differentially stabilize RTK dimers.

Taken together, our results demonstrate that the ligands NT-3, NT-4, and BDNF stabilize dimers with different conformations and different stabilities. Thus, our data support both hypotheses outlined above. Noteworthily, there is no *a priori* reason for the two hypotheses to be mutually exclusive, and in fact, different structures usually have different stabilities. It is possible that the differences in structure and stability of the ligand-bound dimers observed here underlie previously reported differences in the downregulation of Trk-B in response to BDNF and NT-4 (86). BDNF induces more efficient ubiquitination of Trk-B, as compared to NT-4, and targets Trk-B more efficiently to degradative pathways. Our results suggest that the BDNF-bound Trk-B dimer is the most stable one of the three ligand-bound Trk-B dimers. Interestingly, dimers of high stability have been proposed to engage negative feedback mechanisms more efficiently that dimers of lower stabilities (16). This scenario has been proposed for EGFR, and now our results suggest that it may apply to Trk-B as well. Furthermore, it is possible that differences in RTK dimer structure underly the efficiency of its ubiquitination.

This work gives new insights into the biophysical principles that underlie RTK ligand bias. GPCRs transduce biochemical signals across the plasma membrane via conformational changes, and ligand bias occurs when different ligands induce different types of conformational changes. For a long time, RTKs were believed to signal via a fundamentally different mechanism involving ligand-induced lateral dimerization (19). Recently it has become clear, however, that the role of the ligand in RTK activation is more complex, as it also induces conformational changes that are required for efficient RTK signaling

(56,77,87,88). Thus, both dimerization and conformational changes are required for RTK activation in the plasma membrane. Likewise, as shown here, ligand bias can be linked to both ligand-specific dimerization propensities and ligand-specific conformational changes.

## Acknowledgement:

Supported by NIH GM068619

## References

1. Watson J, Arey B, and Alt A (2014) Biased receptor tyrosine kinase signaling pathways. in Biased Signaling in Physiology, Pharmacology, and Therpapeutics (Arey B ed.), Elsevier Inc, NY. pp 137–172
2. Kenakin T (2011) Functional selectivity and biased receptor signaling. J Pharmacol Exp Ther 336, 296–302 [PubMed: 21030484]
3. Kuruvilla R, Zweifel LS, Glebova NO, Lonze BE, Valdez G, Ye HH, and Ginty DD (2004) A neurotrophin signaling cascade coordinates sympathetic neuron development through differential control of TrkA trafficking and retrograde signaling. Cell 118, 243–255 [PubMed: 15260993]
4. Ehlert FJ (2018) Analysis of Biased Agonism. Prog Mol Biol Transl Sci 160, 63–104 [PubMed: 30470293]
5. Kenakin T, and Christopoulos A (2013) Signalling bias in new drug discovery: detection, quantification and therapeutic impact. Nat Rev Drug Discov 12, 205–216 [PubMed: 23411724]
6. Smith JS, Lefkowitz RJ, and Rajagopal S (2018) Biased signalling: from simple switches to allosteric microprocessors. Nat Rev Drug Discov 17, 243–260 [PubMed: 29302067]
7. Wacker D, Wang C, Katritch V, Han GW, Huang XP, Vardy E, McCorvy JD, Jiang Y, Chu M, Siu FY, Liu W, Xu HE, Cherezov V, Roth BL, and Stevens RC (2013) Structural features for functional selectivity at serotonin receptors. Science 340, 615–619 [PubMed: 23519215]
8. Kahsai AW, Xiao K, Rajagopal S, Ahn S, Shukla AK, Sun J, Oas TG, and Lefkowitz RJ (2011) Multiple ligand-specific conformations of the beta2-adrenergic receptor. Nat Chem Biol 7, 692–700 [PubMed: 21857662]
9. Liu JJ, Horst R, Katritch V, Stevens RC, and Wuthrich K (2012) Biased signaling pathways in beta2-adrenergic receptor characterized by 19F-NMR. Science 335, 1106–1110 [PubMed: 22267580]
10. Kenakin T (2017) Signaling bias in drug discovery. Expert Opin Drug Discov 12, 321–333 [PubMed: 28277840]
11. Kenakin T (2019) Biased Receptor Signaling in Drug Discovery. Pharmacol Rev 71, 267–315 [PubMed: 30914442]
12. Correll CC, and McKittrick BA (2014) Biased ligand modulation of seven transmembrane receptors (7TMRs): functional implications for drug discovery. J Med Chem 57, 6887–6896 [PubMed: 24697360]
13. Wisler JW, Rockman HA, and Lefkowitz RJ (2018) Biased G Protein-Coupled Receptor Signaling: Changing the Paradigm of Drug Discovery. Circulation 137, 2315–2317 [PubMed: 29844068]
14. Hidai C, Masako O, Ikeda H, Nagashima H, Matsuoka R, Quertermous T, Kasanuki H, Kokubun S, and Kawana M (2003) FGF-1 enhanced cardiogenesis in differentiating embryonal carcinoma cell cultures, which was opposite to the effect of FGF-2. Journal of Molecular and Cellular Cardiology 35, 421–425 [PubMed: 12689822]
15. Wilson KJ, Gilmore JL, Foley J, Lemmon MA, and Riese DJ 2nd. (2009) Functional selectivity of EGF family peptide growth factors: implications for cancer. Pharmacol Ther 122, 1–8 [PubMed: 19135477]
16. Freed DM, Bessman NJ, Kiyatkin A, Salazar-Cavazos E, Byrne PO, Moore JO, Valley CC, Ferguson KM, Leahy DJ, Lidke DS, and Lemmon MA (2017) EGFR Ligands Differentially Stabilize Receptor Dimers to Specify Signaling Kinetics. Cell 171, 683–695 e618 [PubMed: 28988771]

17. Schlessinger J (2000) Cell signaling by receptor tyrosine kinases. Cell 103, 211–225 [PubMed: 11057895]
18. Lemmon MA, and Schlessinger J (2010) Cell Signaling by Receptor Tyrosine Kinases. Cell 141, 1117–1134 [PubMed: 20602996]
19. Fantl WJ, Johnson DE, and Williams LT (1993) Signaling by Receptor Tyrosine Kinases. Annual Review of Biochemistry 62, 453–481
20. Arteaga CL, and Engelman JA (2014) ERBB receptors: from oncogene discovery to basic science to mechanism-based cancer therapeutics. Cancer Cell 25, 282–303 [PubMed: 24651011]
21. Belov AA, and Mohammadi M (2013) Molecular mechanisms of fibroblast growth factor signaling in physiology and pathology. Cold Spring Harb Perspect Biol 5
22. Wagner MJ, Stacey MM, Liu BA, and Pawson T (2013) Molecular mechanisms of SH2- and PTB-domain-containing proteins in receptor tyrosine kinase signaling. Cold Spring Harb Perspect Biol 5, a008987 [PubMed: 24296166]
23. Sweeney C, Lai C, Riese DJ 2nd, Diamonti AJ, Cantley LC, and Carraway KL 3rd (2000) Ligand discrimination in signaling through an ErbB4 receptor homodimer. The Journal of biological chemistry 275, 19803–19807 [PubMed: 10867024]
24. Hidai C, Masako O, Ikeda H, Nagashima H, Matsuoka R, Quertermous T, Kasanuki H, Kokubun S, and Kawana M (2003) FGF-1 enhanced cardiogenesis in differentiating embryonal carcinoma cell cultures, which was opposite to the effect of FGF-2. J Mol Cell Cardiol 35, 421–425 [PubMed: 12689822]
25. Jorgensen C, Sherman A, Chen GI, Pasculescu A, Poliakov A, Hsiung M, Larsen B, Wilkinson DG, Linding R, and Pawson T (2009) Cell-specific information processing in segregating populations of Eph receptor ephrin-expressing cells. Science 326, 1502–1509 [PubMed: 20007894]
26. Sciacca L, Cassarino MF, Genua M, Pandini G, Le Moli R, Squatrito S, and Vigneri R (2010) Insulin analogues differently activate insulin receptor isoforms and post-receptor signalling. Diabetologia 53, 1743–1753 [PubMed: 20424816]
27. Jensen M, Hansen B, De Meyts P, Schaffer L, and Urso B (2007) Activation of the insulin receptor by insulin and a synthetic peptide leads to divergent metabolic and mitogenic signaling and responses. J Biol Chem 282, 35179–35186 [PubMed: 17925406]
28. Lu C, Mi LZ, Grey MJ, Zhu J, Graef E, Yokoyama S, and Springer TA (2010) Structural evidence for loose linkage between ligand binding and kinase activation in the epidermal growth factor receptor. Mol Cell Biol 30, 5432–5443 [PubMed: 20837704]
29. Lu C, Mi LZ, Schurpf T, Walz T, and Springer TA (2012) Mechanisms for kinase-mediated dimerization of the epidermal growth factor receptor. The Journal of biological chemistry 287, 38244–38253 [PubMed: 22988250]
30. Zinkle A, and Mohammadi M (2018) A threshold model for receptor tyrosine kinase signaling specificity and cell fate determination. F1000Res 7
31. Meakin SO, and Shooter EM (1992) The nerve growth factor family of receptors. Trends Neurosci 15, 323–331 [PubMed: 1382329]
32. Sasahira T, Ueda N, Yamamoto K, Bhawal UK, Kurihara M, Kirita T, and Kuniyasu H (2013) Trks are novel oncogenes involved in the induction of neovascularization, tumor progression, and nodal metastasis in oral squamous cell carcinoma. Clinical & Experimental Metastasis 30, 165–176 [PubMed: 22886570]
33. Bothwell M (2016) Recent advances in understanding neurotrophin signaling. F1000Res 5
34. Zampieri N, and Chao MV (2006) Mechanisms of neurotrophin receptor signalling. Biochem Soc Trans 34, 607–611 [PubMed: 16856873]
35. Yano H, Cong F, Birge RB, Goff SP, and Chao MV (2000) Association of the Abl tyrosine kinase with the Trk nerve growth factor receptor. J Neurosci Res 59, 356–364 [PubMed: 10679771]
36. Chao MV, Rajagopal R, and Lee FS (2006) Neurotrophin signalling in health and disease. Clin Sci (Lond) 110, 167–173 [PubMed: 16411893]
37. Uren RT, and Turnley AM (2014) Regulation of neurotrophin receptor (Trk) signaling: suppressor of cytokine signaling 2 (SOCS2) is a new player. Front Mol Neurosci 7, 39 [PubMed: 24860421]

38. Klein R, Conway D, Parada LF, and Barbacid M (1990) The Trkb Tyrosine Protein-Kinase Gene Codes for a 2nd Neurogenic Receptor That Lacks the Catalytic Kinase Domain. Cell 61, 647–656 [PubMed: 2160854]
39. Klein R, Parada LF, Coulier F, and Barbacid M (1989) Trkb, a Novel Tyrosine Protein-Kinase Receptor Expressed during Mouse Neural Development. Embo Journal 8, 3701–3709
40. Bramham CR, and Messaoudi E (2005) BDNF function in adult synaptic plasticity: The synaptic consolidation hypothesis. Prog Neurobiol 76, 99–125 [PubMed: 16099088]
41. Ohira K, and Hayashi M (2009) A New Aspect of the TrkB Signaling Pathway in Neural Plasticity. Curr Neuropharmacol 7, 276–285 [PubMed: 20514207]
42. Xu BJ, Gottschalk W, Chow A, Wilson RI, Schnell E, Zang KL, Wang DA, Nicoll RA, Lu B, and Reichardt LF (2000) The role of brain-derived neurotrophic factor receptors in the mature hippocampus: Modulation of long-term potentiation through a presynaptic mechanism involving TrkB. Journal of Neuroscience 20, 6888–6897 [PubMed: 10995833]
43. Gupta VK, You YY, Gupta VB, Klistorner A, and Graham SL (2013) TrkB Receptor Signalling: Implications in Neurodegenerative, Psychiatric and Proliferative Disorders. International Journal of Molecular Sciences 14, 10122–10142 [PubMed: 23670594]
44. Soppet D, Escandon E, Maragos J, Middlemas DS, Reid SW, Blair J, Burton LE, Stanton BR, Kaplan DR, Hunter T, Nikolics K, and Parada LF (1991) The neurotrophic factors brain-derived neurotrophic factor and neurotrophin-3 are ligands for the trkB tyrosine kinase receptor. Cell 65, 895–903 [PubMed: 1645620]
45. Wong V, Arriaga R, Ip NY, and Lindsay RM (1993) The Neurotrophins Bdnf, Nt-3 and Nt-4/5, but Not Ngf, up-Regulate the Cholinergic Phenotype of Developing Motor-Neurons. Eur J Neurosci 5, 466–474 [PubMed: 7505167]
46. Philo J, Talvenheimo J, Wen J, Rosenfeld R, Welcher A, and Arakawa T (1994) Interactions of Neurotrophin-3 (Nt-3), Brain-Derived Neurotrophic Factor (Bdnf), and the Nt-3 Bdnf Heterodimer with the Extracellular Domains of the Trkb and Trkc Receptors. Journal of Biological Chemistry 269, 27840–27846
47. Banfield MJ, Naylor RL, Robertson AGS, Allen SJ, Dawbarn D, and Brady RL (2001) Specificity in Trk receptor : neurotrophin interactions: The crystal structure of TrkB-d5 in complex with neurotrophin-4/5. Structure 9, 1191–1199 [PubMed: 11738045]
48. Naylor RL, Robertson AGS, Allen SJ, Sessions RB, Clarke AR, Mason GGF, Burston JJ, Tyler SJ, Wilcock GK, and Dawbarn D (2002) A discrete domain of the human TrkB receptor defines the binding sites for BDNF and NT-4. Biochemical and Biophysical Research Communications 291, 501–507 [PubMed: 11855816]
49. Hall J, Thomas KL, and Everitt BJ (2000) Rapid and selective induction of BDNF expression in the hippocampus during contextual learning. Nature Neuroscience 3, 533–535 [PubMed: 10816306]
50. Fan G, Egles C, Sun Y, Minichiello L, Renger JJ, Klein R, Liu GS, and Jaenisch R (2000) Knocking the NT4 gene into the BDNF locus rescues BDNF deficient mice and reveals distinct NT4 and BDNF activities. Nature Neuroscience 3, 350–357 [PubMed: 10725924]
51. Erickson JT, Conover JC, Borday V, Champagnat J, Barbacid M, Yancopoulos G, and Katz DM (1996) Mice lacking brain-derived neurotrophic factor exhibit visceral sensory neuron losses distinct from mice lacking NT4 and display a severe developmental deficit in control of breathing. Journal of Neuroscience 16, 5361–5371 [PubMed: 8757249]
52. Ip NY, Stitt TN, Tapley P, Klein R, Glass DJ, Fandl J, Greene LA, Barbacid M, and Yancopoulos GD (1993) Similarities and differences in the way neurotrophins interact with the Trk receptors in neuronal and nonneuronal cells. Neuron 10, 137–149 [PubMed: 7679912]
53. Ip NY, Ibanez CF, Nye SH, Mcclain J, Jones PF, Gies DR, Belluscio L, Lebeau MM, Espinosa R, Squinto SP, Persson H, and Yancopoulos GD (1992) Mammalian Neurotrophin-4 - Structure, Chromosomal Localization, Tissue Distribution, and Receptor Specificity. Proceedings of the National Academy of Sciences of the United States of America 89, 3060–3064 [PubMed: 1313578]
54. King C, Stoneman M, Raicu V, and Hristova K (2016) Fully quantified spectral imaging reveals in vivo membrane protein interactions. Integr.Biol.(Camb.) 8, 216–229 [PubMed: 26787445]

55. Sarabipour S, and Hristova K (2016) Mechanism of FGF receptor dimerization and activation. Nat.Commun 7, 10262 [PubMed: 26725515]
56. Ahmed F, and Hristova K (2018) Dimerization of the Trk receptors in the plasma membrane: effects of their cognate ligands. The Biochemical journal 457, 3669–3685
57. Sarabipour S, King C, and Hristova K (2014) Un-induced high-yield bacterial expression of fluorescent proteins. Anal.Biochem. 449, 155–157 [PubMed: 24378720]
58. Sinha B, Koster D, Ruez R, Gonnord P, Bastiani M, Abankwa D, Stan RV, Butler-Browne G, Vedie B, Johannes L, Morone N, Parton RG, Raposo G, Sens P, Lamaze C, and Nassoy P (2011) Cells respond to mechanical stress by rapid disassembly of caveolae. Cell. 144, 402–413 [PubMed: 21295700]
59. Biener G, Stoneman MR, Acbas G, Holz JD, Orlova M, Komarova L, Kuchin S, and Raicu V (2014) Development and Experimental Testing of an Optical Micro-Spectroscopic Technique Incorporating True Line-Scan Excitation. International Journal of Molecular Sciences 15, 261–276
60. King C, Raicu V, and Hristova K (2017) Understanding the FRET Signatures of Interacting Membrane Proteins. The Journal of biological chemistry 292, 5291–5310 [PubMed: 28188294]
61. Chen LR, Novicky L, Merzlyakov M, Hristov T, and Hristova K (2010) Measuring the Energetics of Membrane Protein Dimerization in Mammalian Membranes. Journal of the American Chemical Society 132, 3628–3635 [PubMed: 20158179]
62. Singh DR, Ahmed F, Sarabipour S, and Hristova K (2017) Intracellular Domain Contacts Contribute to Ecadherin Constitutive Dimerization in the Plasma Membrane. J Mol Biol 429, 2231–2245 [PubMed: 28549925]
63. Adámková L, Kvíčalová Z, Rozbeský D, Kukačka Z, Adámek D, Cebecauer M, and Novák P (2019) Oligomeric Architecture of Mouse Activating Nkrp1 Receptors on Living Cells. International journal of molecular sciences 20, 1884
64. Trullo A, Corti V, Arza E, Caiolfa VR, and Zamai M (2013) Application limits and data correction in number of molecules and brightness analysis. Microsc Res Tech 76, 1135–1146 [PubMed: 23934660]
65. Digman MA, Dalal R, Horwitz AF, and Gratton E (2008) Mapping the number of molecules and brightness in the laser scanning microscope. Biophys J 94, 2320–2332 [PubMed: 18096627]
66. Singh DR, Kanvinde P, King C, Pasquale EB, and Hristova K (2018) The EphA2 receptor is activated through induction of distinct, ligand-dependent oligomeric structures. Communications Biology 1, 15 [PubMed: 30271902]
67. Singh DR, Cao Q, King C, Salotto M, Ahmed F, Zhou XY, Pasquale EB, and Hristova K (2015) Unliganded EphA3 dimerization promoted by the SAM domain. Biochemical Journal 471, 101–109
68. Singh DR, Ahmed F, Paul MD, Gedam M, Pasquale EB, and Hristova K (2016) The SAM domain inhibits EphA2 interactions in the plasma membrane. Biochim Biophys Acta
69. Wolber PK, and Hudson BS (1979) An analytic solution to the F”rster energy transfer problem in two dimensions. Biophysical Journal 28, 197–210 [PubMed: 262548]
70. King C, Sarabipour S, Byrne P, Leahy DJ, and Hristova K (2014) The FRET signatures of non-interacting proteins in membranes: simulations and experiments. Biophysical Journal 106, 1309–1317 [PubMed: 24655506]
71. Needham SR, Roberts SK, Arkhipov A, Mysore VP, Tynan CJ, Zanetti-Domingues LC, Kim ET, Losasso V, Korovesis D, Hirsch M, Rolfe DJ, Clarke DT, Winn MD, Lajevardipour A, Clayton AH, Pike LJ, Perani M, Parker PJ, Shan Y, Shaw DE, and Martin-Fernandez ML (2016) EGFR oligomerization organizes kinase-active dimers into competent signalling platforms. Nat Commun 7, 13307 [PubMed: 27796308]
72. Perumal V, Krishnan K, Gratton E, Dharmarajan AM, and Fox SA (2015) Number and brightness analysis of sFRP4 domains in live cells demonstrates vesicle association signal of the NLD domain and dynamic intracellular responses to Wnt3a. Int J Biochem Cell Biol 64, 91–96 [PubMed: 25805505]
73. Plotegher N, Gratton E, and Bubacco L (2014) Number and Brightness analysis of alpha-synuclein oligomerization and the associated mitochondrial morphology alterations in live cells. Biochim Biophys Acta 1840, 2014–2024 [PubMed: 24561157]

74. Digman MA, Stakic M, and Gratton E (2013) Raster Image Correlation Spectroscopy and Number and Brightness Analysis. Fluorescence Fluctuation Spectroscopy (Ffs), Pt A 518, 121–144
75. Sarabipour S, Del Piccolo N, and Hristova K (2015) Characterization of Membrane Protein Interactions in Plasma Membrane Derived Vesicles with Quantitative Imaging Forster Resonance Energy Transfer. Acc.Chem.Res. 48, 2262–2269 [PubMed: 26244699]
76. Wilson KJ, Gilmore JL, Foley J, Lemmon MA, and Riese DJ (2009) Functional selectivity of EGF family peptide growth factors: Implications for cancer. Pharmacology & Therapeutics 122, 1–8 [PubMed: 19135477]
77. Paul MD, and Hristova K (2019) The transition model of RTK activation: A quantitative framework for understanding RTK signaling and RTK modulator activity. Cytokine Growth Factor Rev 49, 23–31 [PubMed: 31711797]
78. Sarabipour S, Ballmer-Hofer K, and Hristova K (2016) VEGFR-2 conformational switch in response to ligand binding. Elife 5
79. Scheck RA, Lowder MA, Appelbaum JS, and Schepartz A (2012) Bipartite tetracysteine display reveals allosteric control of ligand-specific EGFR activation. ACS Chem Biol 7, 1367–1376 [PubMed: 22667988]
80. Doerner A, Scheck R, and Schepartz A (2015) Growth Factor Identity Is Encoded by Discrete Coiled-Coil Rotamers in the EGFR Juxtamembrane Region. Chem.Biol. 22, 776–784 [PubMed: 26091170]
81. Kobashigawa Y, Amano S, Yokogawa M, Kumeta H, Morioka H, Inouye M, Schlessinger J, and Inagaki F (2015) Structural analysis of the mechanism of phosphorylation of a critical autoregulatory tyrosine residue in FGFR1 kinase domain. Genes Cells 20, 860–870 [PubMed: 26300540]
82. Bae JH, Boggon TJ, Tome F, Mandiyan V, Lax I, and Schlessinger J (2010) Asymmetric receptor contact is required for tyrosine autophosphorylation of fibroblast growth factor receptor in living cells. Proceedings of the National Academy of Sciences of the United States of America 107, 2866–2871 [PubMed: 20133753]
83. Chen L, Marsiglia WM, Chen H, Katigbak J, Erdjument-Bromage H, Kemble DJ, Fu L, Ma J, Sun G, Zhang Y, Liang G, Neubert TA, Li X, Traaseth NJ, and Mohammadi M (2020) Molecular basis for receptor tyrosine kinase A-loop tyrosine transphosphorylation. Nat Chem Biol 16, 267–277 [PubMed: 31959966]
84. Chen H, Xu CF, Ma J, Eliseenkova AV, Li W, Pollock PM, Pitteloud N, Miller WT, Neubert TA, and Mohammadi M (2008) A crystallographic snapshot of tyrosine trans-phosphorylation in action. Proc Natl Acad Sci U S A 105, 19660–19665 [PubMed: 19060208]
85. Xu Q, Malecka KL, Fink L, Jordan EJ, Duffy E, Kolander S, Peterson JR, and Dunbrack RL Jr. (2015) Identifying three-dimensional structures of autophosphorylation complexes in crystals of protein kinases. Sci Signal 8, rs13 [PubMed: 26628682]
86. Proenca CC, Song M, and Lee FS (2016) Differential effects of BDNF and neurotrophin 4 (NT4) on endocytic sorting of TrkB receptors. Journal of Neurochemistry 138, 397–406 [PubMed: 27216821]
87. Moriki T, Maruyama H, and Maruyama IN (2001) Activation of preformed EGF receptor dimers by ligand-induced rotation of the transmembrane domain. Journal of Molecular Biology 311, 1011–1026 [PubMed: 11531336]
88. Hyde CA, Giese A, Stuttfeld E, Abram SJ, Villemagne D, Schleier T, Binz HK, and Ballmer-Hofer K (2012) Targeting extracellular domains D4 and D7 of vascular endothelial growth factor receptor 2 reveals allosteric receptor regulatory sites. Molecular and Cellular Biology 32, 3802–3813 [PubMed: 22801374]

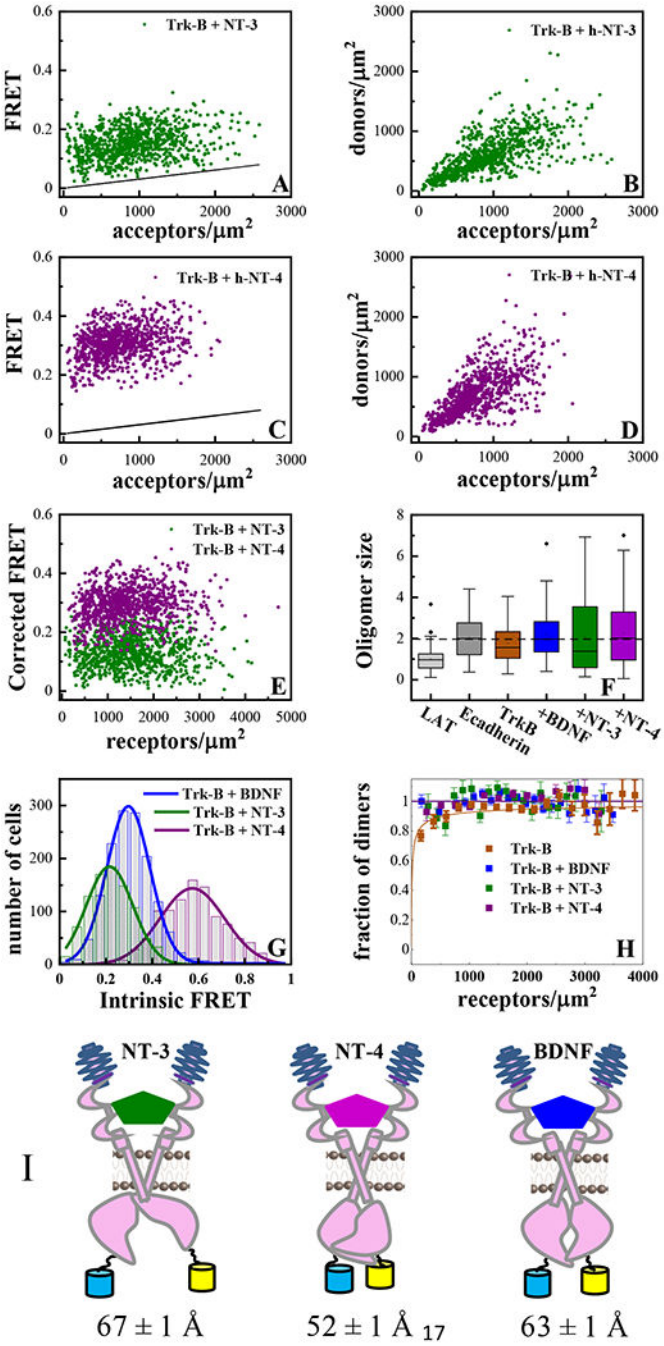


**Figure 1.**

Dimerization of full-length Trk-B in the presence of saturating concentrations (380 nM) of the three ligands. (A) FRET as a function of acceptor concentration for Trk-B in the presence of 380 nM NT-3. The solid black line shows the proximity FRET, which is FRET due to the random close approach of donor and acceptor fluorophores in the membrane. (B) Trk-B-mTurquoise (donor) concentration versus Trk-B-YFP (acceptor) concentration in the presence of NT-3. (C) FRET as a function of acceptor concentration for Trk-B in the presence of NT-4. The proximity FRET is shown with the solid black line. (D) Trk-B-

mTurquoise (donor) concentration versus Trk-B-YFP (acceptor) concentration in the presence of NT-4. (E) FRET, after the correction for proximity FRET (correction procedure described in (60)). The corrected FRET does not depend on the concentration. (F) Number and Brightness measurements of oligomer size of LAT (monomer control), Ecadherin (dimer control), Trk-B in the absence of ligand and in the presence of BDNF, NT-3, and NT-4. (G) Histogram of Trk-B Intrinsic FRET values in the presence of BDNF, NT-3 and NT-4. (H) Trk-B dimerization curves (fraction of dimers as a function of total receptor concentration) in the absence of ligand and in the presence of BDNF, NT-3 and NT-4. The dimerization parameters measured for Trk-B in the presence of the three ligands are reported in Table 1. Data in the absence of ligand and in the presence of BDNF are from (56). (I) Summary of findings. Not drawn to scale, and meant to emphasize measured differences in average distance between fluorescent proteins (see Discussion).

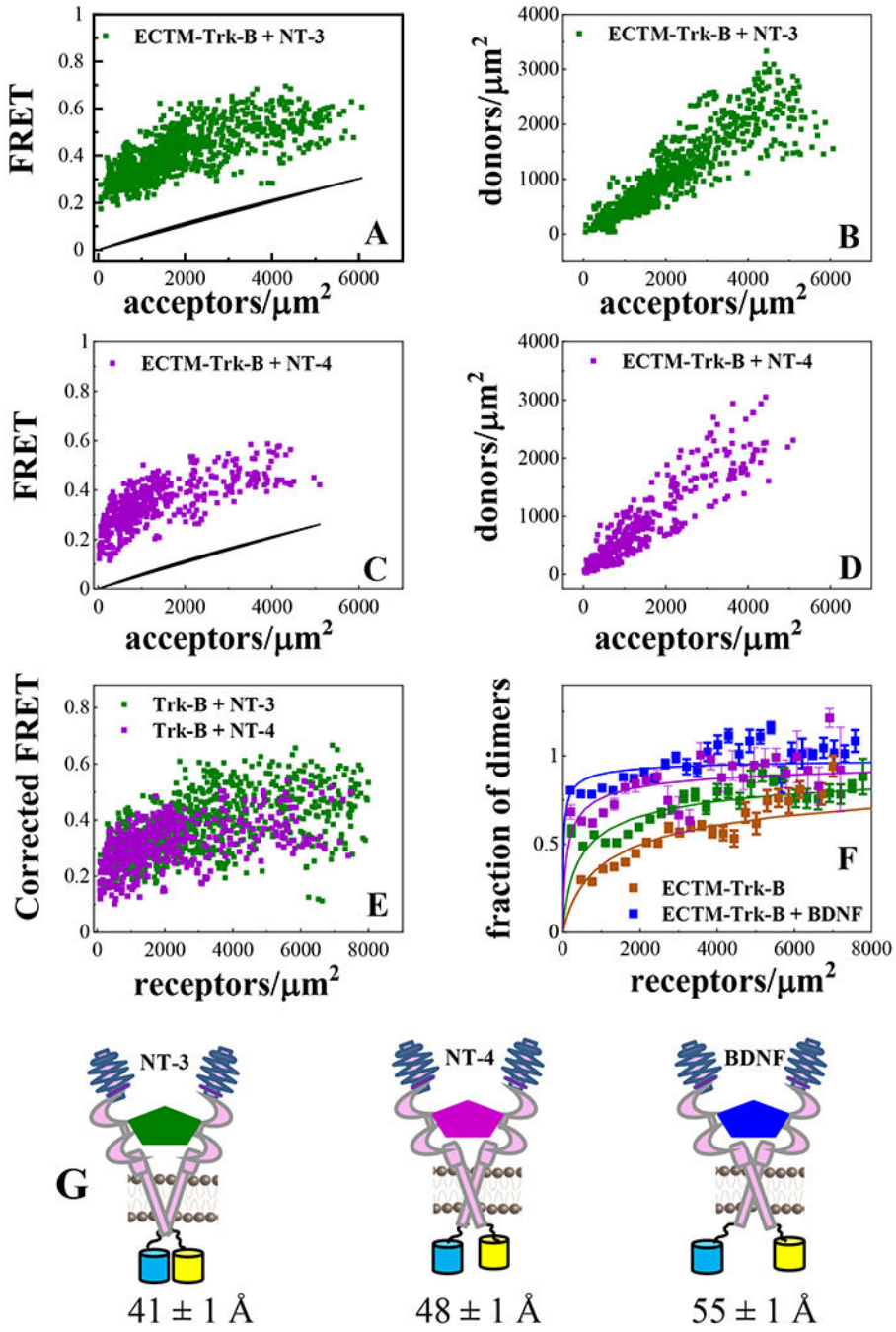


**Figure 2.**

Dimerization of truncated ECTM Trk-B in the presence of saturating concentrations (380 nM) of the three ligands. (A) FRET as a function of acceptor concentration in the presence of 380 nM NT-3. The solid black line shows the proximity FRET. (B) ECTM Trk-B-mTurquoise (donor) concentration versus ECTM Trk-B-YFP (acceptor) concentration in the presence of NT-3. (C) FRET as a function of acceptor concentration in the presence of 380 nM NT-4, along with the proximity FRET contribution. (D) ECTM Trk-B-mTurquoise (donor) concentration versus ECTM Trk-B-YFP (acceptor) concentration in the presence of

NT-4. (E) FRET, after the correction for proximity FRET (correction procedure described in (60). The corrected FRET increases with concentration. (F) ECTM Trk-B dimerization curves (fraction of dimers as a function of concentration) in the absence of ligand and in the presence of 380 nM BDNF, NT-3, and NT-4. The dimerization parameters measured for ECTM Trk-B in the presence of the three ligands are reported in Table 1. Data in the absence of ligand and in the presence of 380 nM BDNF are from (56). (G) Summary of findings. Not drawn to scale, and meant to emphasize measured differences in average distance between fluorescent proteins (see Discussion).

**Table 1.**

Dimerization parameters for full-length and truncated ECTM Trk-B receptors, in the absence of ligand and in the presence of 380 nM NT-3, NT-4, or BDNF. $K_{diss}$ is the two-dimensional dissociation constant, a thermodynamic parameter, which is related to the stability of the Trk-B dimers, $\Delta G$, according to equation (4). $\widetilde{E}$ is the Intrinsic FRET, which depends on the positioning of the fluorescent proteins within the Trk dimers. Differences in Intrinsic FRET in the presence of the three ligands are highly statistically significant ($p<0.001$ from ANOVA). The average distance between the fluorescent proteins, $d$, is calculated from $\widetilde{E}$ using equation (4), under the assumption for free rotation of the fluorescent proteins.

| **Full length** | $K_{diss}$ **(rec.μm$^{-2}$)** | **Δ*G* (kcal/mol)** | **Intrinsic FRET ($\widetilde{E}$)** | ***d*(Å)** |
|---|---|---|---|---|
| Trk-B * | 12 ± 2 | −6.72 ± 0.10 | 0.35 ± 0.04 | 60 ± 2 |
| Trk-B+NT-3 | 100% dimer | n.d. | 0.22 ± 0.02 | 67 ± 1 |
| Trk-B+NT-4 | 100% dimer | n.d. | 0.57 ± 0.02 | 52 ± 1 |
| Trk-B+BDNF * | 100% dimer | n.d. | 0.30 ± 0.02 | 63 ± 1 |
| ECTM Trk-B * | 2018 ± 134 | −3.68 ± 0.04 | 0.82 ± 0.02 | 42 ± 1 |
| ECTM Trk-B+NT-3 | 710 ± 40 | −4.30 ± 0.07 | 0.85 ± 0.02 | 41 ± 1 |
| ECTM Trk-B+NT-4 | 150 ± 36 | −5.22 ± 0.15 | 0.68 ± 0.02 | 48 ± 1 |
| ECTM Trk-B+BDNF * | 23 ± 2 | −6.33 ± 0.06 | 0.50 ± 0.01 | 55 ± 1 |

[a] n.d.: not determined.

* Data in the absence if ligand and in the presence of BDNF are from (56).